Available online at www.sciencedirect.com
ScienceDirect
Journal of Sound and Vibration 313 (2008) 342–359
JOURNAL OF SOUND AND VIBRATION
www.elsevier.com/locate/jsvi

Customized wavelet denoising using intra- and inter-scale dependency for bearing fault detection

Li Zhen[a,*], He Zhengjia[b], Zi Yanyang[a], Wang Yanxue[a]

[a]School of Mechanical Engineering, Xi'an Jiaotong University, 710049 Xi'an, China
[b]State Key Lab for Manufacturing Systems Engineering, Xi'an Jiaotong University, 710049 Xi'an, China

Received 16 December 2006; received in revised form 14 November 2007; accepted 17 November 2007
Available online 27 December 2007

Abstract

Bearing fault detection is a challenging task, especially at the incipient stage. Wavelet denoising is widely recognized as an effective tool for signal processing and feature extraction. The wavelet denoising method by incorporating neighboring coefficients (NeighCoeff), which is proposed by Cai and Silverman, gives the better results than the traditional term-by-term approaches. However, this method only exploits intra-scale dependency of wavelet coefficients. It does not consider the inter-scale dependency of wavelet coefficients. In this paper, customized wavelet denoising using intra- and inter-scale dependency of wavelet coefficients is proposed for bearing fault detection. By designing the prediction operator and update operator, a customized wavelet based on the lifting scheme is constructed directly to match the transient properties of a given signal. The NeighCoeff denoising algorithm is improved by taking into account the intra- and inter-scale dependency of wavelet coefficients. The results of the application to bearing fault detection show that the proposed method is very effective.

1. Introduction

Bearing fault detection is a typical problem in rotating machinery fault diagnosis [1]. Material fatigue, faulty installation, or inappropriate lubrication may cause localized defects of rolling bearings. Each time the rolling element passes over the defect, an impulse of vibration is generated. The periodic impulses in the vibration signals contain rich information about bearing health. However, defect-induced impulses are rather weak at the incipient stage, and often buried in background noise. Therefore, denoising and extraction of the defect-related signals are very important for bearing fault detection.

There are many vibration-based diagnosis techniques available for rolling bearings, for example, statistical analysis [2], adaptive noise canceling [3], high-frequency resonance technique [4], neural network [5], and fuzzy logic [6]. However, there is no ideal way to extract the weak signals of bearing incipient defects. One main reason is that the signal-to-noise ratio (SNR) is lower, and the defect-induced signals are more difficult to be

*Corresponding author. Fax: +86 29 82 663 689.
E-mail address: xjtu_lizhen@163.com (L. Zhen).

0022-460X/$ - see front matter © 2007 Elsevier Ltd. All rights reserved.
doi:10.1016/j.jsv.2007.11.039

Nomenclature

$\boldsymbol{d}^{(0)}$	odd samples of original signal
$\tilde{\boldsymbol{d}}^{(l+1)}$	wavelet coefficients of redundant decomposition at level $l+1$
N	the number of prediction coefficients
$\tilde{N}$	the number of update coefficients
$\boldsymbol{P}$	prediction operator
P_{opt}	optimal prediction operator
$\boldsymbol{P}^{(l)}$	redundant prediction operator at level l
$\boldsymbol{s}^{(0)}$	even samples of original signal
$\tilde{\boldsymbol{s}}^{(l+1)}$	approximation coefficients of redundant decomposition at level $l+1$
$\boldsymbol{U}$	update operator
U_{opt}	optimal update operator
$\boldsymbol{U}^{(l)}$	redundant update operator at level l
$\boldsymbol{x}$	original signal

isolated. Many researchers have investigated the application of wavelet transform to vibration signal analysis for bearing fault detection [7–11]. One common approach taken by the prior studies is that the standard wavelets selected from a library of wavelet functions are used as the mother wavelets. Unfortunately, such standard wavelet functions are independent of a given signal. Since different types of wavelets have different time–frequency structures, it is always very difficult to choose the best wavelet function for feature extraction. Moreover, an inappropriate wavelet will directly decrease the accuracy of the fault detection. To overcome the above limitation, it is necessary to develop new methods to design customized wavelets for machine fault diagnosis. The lifting scheme is developed by Sweldens as a powerful tool to construct biorthogonal wavelets in the spatial domain [12,13]. It provides a great deal of flexibility and freedom for the construction of biorthogonal wavelets, and can be used to construct customized wavelets by the design of prediction operator and update operator. In Refs. [14,15], the lifting scheme has been applied for rotating machinery fault diagnosis.

Wavelet denoising techniques are used to increase the SNR, such as Donoho [16] proposed a simple thresholding rule which sets all the coefficients smaller than the universal threshold $\sigma\sqrt{2\log n}$ to zero and shrinks the rest of the coefficients by the threshold (soft-thresholding) or retains them without change (hard-thresholding). This algorithm offered the advantage of smoothness and adaptation. However, Coifman and Donoho [17] pointed out this algorithm exhibit visual artifacts: Gibbs phenomena in the neighborhood of discontinuities. Therefore, they developed a translation-invariant (TI) denoising scheme to suppress such artifacts. But the traditional term-by-term approaches for both TI and non-TI wavelet denoising do not consider the intra-scale or/and inter-scale dependency of wavelet coefficients. Cai and Silverman [18] proposed a thresholding scheme by taking immediate neighbor coefficients into account. Their experimental results showed that neighboring coefficients (NeighCoeff) thresholding was better than traditional term-by-term wavelet denoising. Chen and Bui [19] extended the NeighCoeff thresholding idea to the multiwavelet case. However, NeighCoeff wavelet thresholding only explored intra-scale dependency. Some new denoising schemes were developed by exploiting the intra- and inter-scale dependency of wavelet coefficients [20–22].

To make up the deficiency of NeighCoeff denoising, a new denoising method based on customized wavelet is proposed in this paper. A customized wavelet is constructed directly by the design of prediction operator and update operator. The genetic algorithms are used to design the prediction operator based on kurtosis maximization principle. The update operator is designed to minimize a reconstruction error. The NeighCoeff denoising method is improved by exploiting the intra- and inter-scale dependency of wavelet coefficients. We find that the customized wavelet denoising using intra- and inter-scale dependency can closely match the characteristics of vibration signals, and it is very effective to capture bearing fault symptoms from the complex vibration signals.

The structure of the paper is organized as follows. In Section 2, the theory of lifting scheme is reviewed briefly. In Section 3, a customized wavelet based on the lifting scheme is set up. In Section 4, we discuss the redundant version of the lifting scheme. Section 5 describes the improved NeighCoeff denoising. In Section 6, the proposed method is applied to detect localized defects of rolling bearings. Conclusions are given in Section 7.

2. Review of the lifting scheme

The lifting scheme is a very general and highly flexible tool to construct biorthogonal wavelets in the spatial domain [12,13]. The lifting scheme consists in three main steps.

In the split step, the original signal $\boldsymbol{x} = (x_i)_{i\in Z}$ is split into even samples $\boldsymbol{s}^{(0)} = (s_i^{(0)})_{i\in \boldsymbol{Z}}$, and odd samples $\boldsymbol{d}^{(0)} = (d_i^{(0)})_{i\in \boldsymbol{Z}}$,

$$s_i^{(0)} = x_{2i}, \quad d_i^{(0)} = x_{2i+1}. \tag{1}$$

In the prediction step, we apply an operator $\boldsymbol{P}$ on $\boldsymbol{s}^{(0)}$ to predict $\boldsymbol{d}^{(0)}$. The prediction error $\boldsymbol{d} = (d_i)_{i\in \boldsymbol{Z}}$ is regarded as wavelet coefficients of $\boldsymbol{x}$,

$$d_i = d_i^{(0)} - \sum_{r=-N/2+1}^{N/2} p_r s_{i+r}^{(0)}, \tag{2}$$

where p_r are coefficients of the prediction operator $\boldsymbol{P}$, and N is the number of prediction coefficients.

In the update step, an update of even samples $\boldsymbol{s}^{(0)}$ is accomplished by using an update operator $\boldsymbol{U}$ on wavelet coefficients $\boldsymbol{d}$ and adding the result to $\boldsymbol{s}^{(0)}$, the update sequence $\boldsymbol{s} = (s_i)_{i\in \boldsymbol{Z}}$ can be regarded as the approximation coefficients of $\boldsymbol{x}$,

$$s_i = s_i^{(0)} + \sum_{j=-\tilde{N}/2+1}^{\tilde{N}/2} u_j d_{i+j-1}, \tag{3}$$

where u_j are coefficients of the update operator $\boldsymbol{U}$, and $\tilde{N}$ is the number of update coefficients.

Let $\boldsymbol{s}$ be the input signal for lifting scheme, the wavelet coefficients and approximation coefficients at the lower resolution can be obtained. The inverse lifting scheme can be immediately performed by reversing the prediction and update operators and changing each '+' into '−' and vice versa. Fig. 1 shows the forward and inverse transform of the lifting scheme.

3. The construction of customized wavelet based on the lifting scheme

The theorems in Ref. [12], expressed by Sweldens in the lifting framework, ensure the biorthogonality of wavelet relevant to the lifting scheme. However, different prediction operator $\boldsymbol{P}$ and update operator $\boldsymbol{U}$ can construct wavelet functions with different time–frequency structures. In order to optimize the prediction operator and update operator, Gouze [23] introduced two meaningful conditions for operator $\boldsymbol{P}$ and $\boldsymbol{U}$. The symmetrical linear phase constraints are expressed as follows:

$$p_r = p_{-r+1}, \quad r = 1, 2, \ldots, N/2, \tag{4}$$

$$u_j = u_{-j+1}, \quad j = 1, 2, \ldots, \tilde{N}/2. \tag{5}$$

The filtering 'normalization' constraints are expressed as follows:

$$\sum_{r=1}^{N/2} p_r = \frac{1}{2}, \tag{6}$$

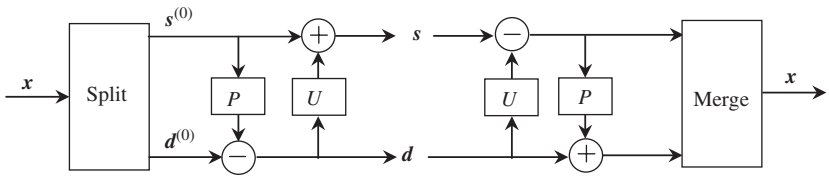

Fig. 1. The forward and inverse transform of the lifting scheme.

$$\sum_{j=1}^{\tilde{N}/2} u_j = \frac{1}{4}. \tag{7}$$

3.1. Design of the optimal prediction operator $\boldsymbol{P}_{opt}$

The prediction step provides the wavelet coefficients $\boldsymbol{d}$. To ensure that the derived wavelet can efficiently isolate the feature components from original signal, a criterion for the prediction operator is needed. Kurtosis is used in engineering to detect fault symptoms because it is sensitive to sharp changed structures, such as impulses [24]. In this paper, we use kurtosis as the performance measure of prediction operator. The criterion of prediction operator $\boldsymbol{P}$ is defined as follows:

$$K_P = \frac{E\{(\boldsymbol{d} - \bar{d})^4\}}{\sigma^4}, \tag{8}$$

where $\bar{d}$ and σ are the mean and standard deviation of wavelet coefficients $\boldsymbol{d}$, and $E\{\cdot\}$ is the expectation. Our objective is to find the optimal prediction operator $\boldsymbol{P}_{\text{opt}}$ that maximizes the kurtosis criterion K_p while satisfying constraints (4) and (6).

Many optimization methods have been presented, and each has its own advantages and limitations. One of the main advantages of genetic algorithms [25] is that it does not have mathematical requirements on the optimization problem. Moreover, genetic algorithms are effective in global optimization. In this paper, genetic algorithms are used to optimize the prediction operator $\boldsymbol{P}$.

In the initialization population for prediction operator $\boldsymbol{P}$, the coefficients $(p_{-N/2+1}, \ldots, p_{N/2})$ of the prediction operator $\boldsymbol{P}$ are coded using the real-coded mechanism. First, the coefficients $(p_2, \ldots, p_{N/2})$ are generated randomly. Second, the coefficients $(p_{-N/2+1}, \ldots, p_{-1})$ are given according to Eq. (4). Finally, the coefficients (p_0, p_1) are obtained by the following formula:

$$p_0 = p_1 = \frac{1}{2} - \sum_{r=2}^{N/2} p_r. \tag{9}$$

The arithmetic crossover and uniform mutation operators commonly used in genetic algorithms were employed for the optimization process [25]. To increase the efficiency of the process, the population scale is set to 50, the number of iteration to 100, the probability of crossover to 0.7 and the probability of mutation to 0.025.

3.2. Design of the optimal update operator $\boldsymbol{U}_{opt}$

An effective update operator provides approximation coefficients, offering an accurate representation of the original signal at the lower resolution. To obtain the optimal update coefficients, the quadratic error of reconstruction [23] is used as the criterion. It is described as follows:

$$J_U = E\{(\hat{\boldsymbol{s}}^{(0)} - \boldsymbol{s}^{(0)})^2\} + E\{(\hat{\boldsymbol{d}}^{(0)} - \boldsymbol{d}^{(0)})^2\}, \tag{10}$$

where $\hat{\boldsymbol{s}}^{(0)}$ and $\hat{\boldsymbol{d}}^{(0)}$ represent even samples and odd samples of the reconstructed signal $\hat{\boldsymbol{x}}$ without using wavelet coefficients $\boldsymbol{d}$. When $\boldsymbol{d} = 0$, the inverse lifting scheme is shown in Fig. 2.

From Fig. 2, $\hat{\boldsymbol{s}}^{(0)}$ and $\hat{\boldsymbol{d}}^{(0)}$ are given by the following equations:

$$\hat{\boldsymbol{s}}^{(0)} = \boldsymbol{s}, \tag{11}$$

$$\hat{\boldsymbol{d}}^{(0)} = \boldsymbol{P}\boldsymbol{s}. \tag{12}$$

During the design of the update operator, our goal is to find the optimal update operator $\boldsymbol{U}_{\text{opt}}$ that could minimize the criterion J_U while satisfying constraints (5) and (7).

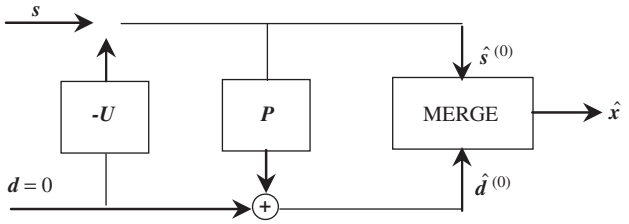

Fig. 2. The inverse lifting scheme with $\boldsymbol{d} = 0$.

Let λ be the Lagrange operator, under constraint (7), the new criterion can be expressed as follows:

$$J_U(u,\lambda) = E\{(\hat{\boldsymbol{s}}^{(0)} - \boldsymbol{s}^{(0)})^2\} + E\{(\hat{\boldsymbol{d}}^{(0)} - \boldsymbol{d}^{(0)})^2\} + \lambda\left(\frac{1}{4} - \sum_{j=1}^{\tilde{N}/2} u_j\right). \tag{13}$$

Considering Eqs. (3), (5), and (11), we obtain

$$E\{(\hat{\boldsymbol{s}}^{(0)} - \boldsymbol{s}^{(0)})^2\} = E\left\{\left[\sum_{j=1}^{\tilde{N}/2} u_j(d_{i+j-1} + d_{i-j})\right]^2\right\}. \tag{14}$$

From Eqs. (2), (3), (5), and (12), we deduce the following result:

$$E\{(\hat{\boldsymbol{d}}^{(0)} - \boldsymbol{d}^{(0)})^2\} = E\left\{\left[\sum_{j=1}^{\tilde{N}/2} u_j(s'_{i+j} + s'_{i-j+1}) - d_i\right]^2\right\}, \tag{15}$$

where

$$s'_i = \sum_{r=1}^{N/2} p_r(d_{i-r} + d_{i+r-1}). \tag{16}$$

To minimize Eq. (13), partial derivatives of the criterion $J_U(u, \lambda)$ with respect to the variable u_j and λ are expressed as follows:

$$\frac{\partial J_U(u,\lambda)}{\partial u_j} = 0, \quad j = 1, 2, \ldots, \tilde{N}/2, \tag{17}$$

$$\frac{\partial J_U(u,\lambda)}{\partial \lambda} = 0. \tag{18}$$

By setting

$$A_{k,l} = E\{(d_{i+k-1} + d_{i-k})(d_{i+l-1} + d_{i-l}) + (s'_{i+k} + s'_{i-k+1})(s'_{i+l} + s'_{i-l+1})\}, \tag{19}$$

$$B_{k,1} = E\{d_i(s'_{i+k} + s'_{i-k+1})\}. \tag{20}$$

A linear system with $(\tilde{N}/2 + 1)$ variables, which is combined by Eqs. (17) and (18), can be rewritten as

$$\mathbf{AY} = \mathbf{B} \tag{21}$$

with

$$\mathbf{A} = \begin{bmatrix} A_{1,1} & \cdots & A_{1,\tilde{N}/2} & -1 \\ \vdots & \ddots & \vdots & \vdots \\ A_{\tilde{N}/2,1} & \cdots & A_{\tilde{N}/2,\tilde{N}/2} & -1 \\ 1 & \cdots & 1 & 0 \end{bmatrix}, \tag{22}$$

$$\mathbf{Y} = [u_1, \ldots, u_{\tilde{N}/2}, \lambda]^{\mathrm{T}}, \tag{23}$$

$$\mathbf{B} = [B_{1,1}, \ldots, B_{\tilde{N}/2,1}, 1/4]^{\mathrm{T}}. \tag{24}$$

According to Eq. (5) and the vector $\mathbf{Y} = [u_1, u_2, \ldots, u_{\tilde{N}/2}, \lambda]$, we can obtain the optimal update operator $\boldsymbol{U}_{\mathrm{opt}} = [u_{-\tilde{N}/2+1}, \ldots, u_0, u_1, \ldots, u_{\tilde{N}/2}]$.

4. The redundant lifting scheme

For the classical wavelet transform, a solution for translation invariance is given by redundant wavelet transform, which eliminates the decimation step and retains the information of low- and high-frequency signals. The redundant wavelet transform can also be translated into a redundant lifting scheme [26]. The forward and inverse transform of redundant lifting scheme is shown in Fig. 3.

Based on the design of customized wavelet mentioned in Section 3, we obtain the prediction operator $\boldsymbol{P}_{\mathrm{opt}}$ and update operator $\boldsymbol{U}_{\mathrm{opt}}$, which closely match the inspected signal. In the redundant lifting scheme, the split step is discarded. The redundant prediction operator $\boldsymbol{P}^{(l)}$ and the redundant update operator $\boldsymbol{U}^{(l)}$ are computed by padding the prediction operator $\boldsymbol{P}_{\mathrm{opt}}$ and update operator $\boldsymbol{U}_{\mathrm{opt}}$ with zeros at the corresponding level l. The decomposition results of an approximation signal $\tilde{\boldsymbol{s}}^{(l)}$ at level l with redundant lifting scheme are expressed by following equations:

$$\tilde{\boldsymbol{d}}^{(l+1)} = \tilde{\boldsymbol{s}}^{(l)} - \boldsymbol{P}^{(l)}\tilde{\boldsymbol{s}}^{(l)}, \tag{25}$$

$$\tilde{\boldsymbol{s}}^{(l+1)} = \tilde{\boldsymbol{s}}^{(l)} + \boldsymbol{U}^{(l)}\tilde{\boldsymbol{d}}^{(l+1)}, \tag{26}$$

where $\tilde{\boldsymbol{d}}^{(l+1)}$ and $\tilde{\boldsymbol{s}}^{(l+1)}$ are wavelet coefficients and approximation coefficients at level $l+1$.

5. The wavelet denoising based on intra- and inter-scale dependency

The basic motivation of NeighCoeff thresholding is that if the current coefficient contains some signal, then it is likely that the two neighbor coefficients also do. For this reason, Cai and Silverman [18] proposed the following thresholding scheme for wavelet denoising. If $S_{l,i}^2 = (\tilde{d}_{i-1}^{(l)})^2 + (\tilde{d}_i^{(l)})^2 + (\tilde{d}_{i+1}^{(l)})^2$ is less than or equal to λ^2, then we set the wavelet coefficient $\tilde{d}_i^{(l)}$ to zero. Otherwise, we set it to

$$\tilde{d}_i^{(l)} = \tilde{d}_i^{(l)}\left(1 - \frac{\mu_l^2}{S_{l,i}^2}\right), \tag{27}$$

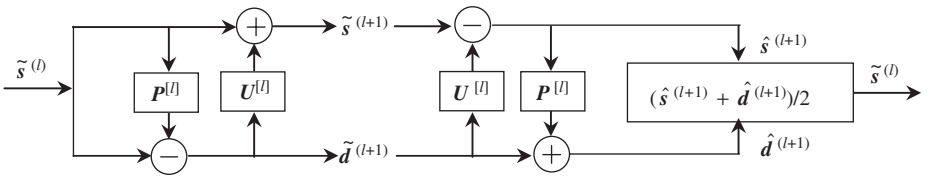

Fig. 3. The forward and inverse transform of redundant lifting scheme.

where $\mu_l = \sqrt{2\sigma_l^2 \log n}$, l is the scale level. n and σ denotes the length and standard deviation of wavelet coefficients $\tilde{\boldsymbol{d}}^{(l)}$, respectively. It should be mentioned that if $\tilde{d}_i^{(l)}$ is at the left (right) boundary of wavelet coefficients, we omit the first (last) term in $S_{l,i}^2$.

It is well known that wavelet coefficients are dependent [27] due to two properties of wavelet transform: (1) a coefficient is large or small, the adjacent coefficients are likely to be large or small, and (2) large or small coefficients tend to propagate across the scales. The NeighCoeff thresholding scheme exploits the intra-scale dependency of wavelet coefficients. However, this method does not consider the evolution of wavelet coefficients along scale, which usually carries important information. In this paper, we improve the NeighCoeff thresholding algorithm using intra- and inter-scale dependency of wavelet coefficients. As observed as Xu et al. [20], the two or three consecutive resolutions can obtain better results than more consecutive resolutions. Therefore, the NeighCoeff thresholding scheme is improved by the following method.

Suppose $S_{l+1,i}^2 = (\tilde{d}_{i-1}^{(l+1)})^2 + (\tilde{d}_i^{(l+1)})^2 + (\tilde{d}_{i+1}^{(l+1)})^2$, let $\mu_{l+1} = \sqrt{2\sigma_{l+1}^2 \log n}$ be the threshold of wavelet coefficients $\tilde{\boldsymbol{d}}^{(l+1)}$ at level $l+1$. Then the improved thresholding formula is given by

$$\tilde{d}_{l,i} = \begin{cases} \tilde{d}_{l,i}\left(1 - \dfrac{\mu_l^2 + \mu_{l+1}^2}{S_{l,i}^2 + S_{l+1,i}^2}\right) & \text{if } S_{l,i}^2 + S_{l+1,i}^2 \geqslant \mu_l^2 + \mu_{l+1}^2, \\ 0 & \text{otherwise.} \end{cases} \tag{28}$$

The customized wavelet denoising using the intra- and intra-scale dependency of wavelet coefficients can be summarized as follows:

(1) Calculate the optimal prediction operator $\boldsymbol{P}_{\text{opt}}$ and the optimal update operator $\boldsymbol{U}_{\text{opt}}$, and construct the customized wavelet.
(2) Perform the decomposition of redundant lifting scheme, obtaining the wavelet coefficients $\tilde{\boldsymbol{d}}^{(l)}$, $\tilde{\boldsymbol{d}}^{(l+1)}$.
(3) Compute the parameters $S_{l,i}^2, S_{l+1,i}^2$ and the thresholds μ_l, μ_{l+1}.
(4) Apply the improved algorithm Eq. (28) to modify wavelet coefficients $\tilde{d}_i^{(l)}$.
(5) Obtain the reconstruction signal using the inverse transform of redundant lifting scheme.

6. The proposed denoising scheme for bearing fault detecting

6.1. Simulation experiment

To verify the feasibility of the proposed method for the extraction of the weak signals, an impulse signal is described as $0.2e^{-200t}\sin(5000t)$ and a simulated signal is composed of periodic impulse signals with a period of 0.12 s. The sampling frequency is 2000 Hz. Fig. 4 shows the simulated signal. The simulated signal is contaminated with additive white noise. The noise level is defined as the ratio of the energy of the white noise to the energy of the periodic impulse signal. The noise ratio is 12.68. The noisy signal is shown in Fig. 5. The impulse components are masked by the noise, we can hardly find any periodic impulses in Fig. 5. The customized wavelet denoising using the intra- and inter-scale dependency is applied to analyze the noisy signal. The optimal prediction operator and update operator are $\boldsymbol{P}_{\text{opt}} = [0.2741, -0.4385, 0.6644, 0.6644, -0.4385, 0.2741]$, $\boldsymbol{U}_{\text{opt}} = [0.0142, -0.0030, 0.2388, 0.2388, -0.0030, 0.0142]$. The customized scaling function and wavelet function are shown in Fig. 6. The noisy signal is performed 4-level decomposition by redundant lifting scheme, and then the wavelet coefficients are thresholded by our improved algorithm. The purified signal using the proposed method is shown in Fig. 7(a). Evenly spaced impulse clusters can be observed from Fig. 7(a). The Donoho's hard-thresholding, soft-thresholding and NeighCoeff denoising based on non-adaptive lifting scheme are also applied to analyze the same signal for comparison. In the non-adaptive lifting scheme, the prediction operator and update operator, which are independent of the inspected signal, are obtained by the interpolation subdivision method introduced in Ref. [28]. They are [0.0117, −0.0977, 0.5859, 0.5859, −0.0977, 0.0117], and [0.0059, −0.0488, 0.2930, 0.2930, −0.0488, 0.0059], respectively. The purified signals using Donoho's hard-thresholding, Donoho's soft-thresholding and NeighCoeff denoising are shown in Fig. 7.

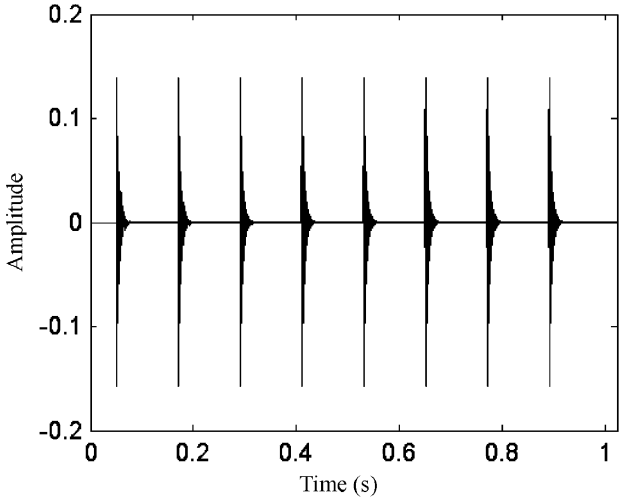

Fig. 4. The simulated impulse signals.

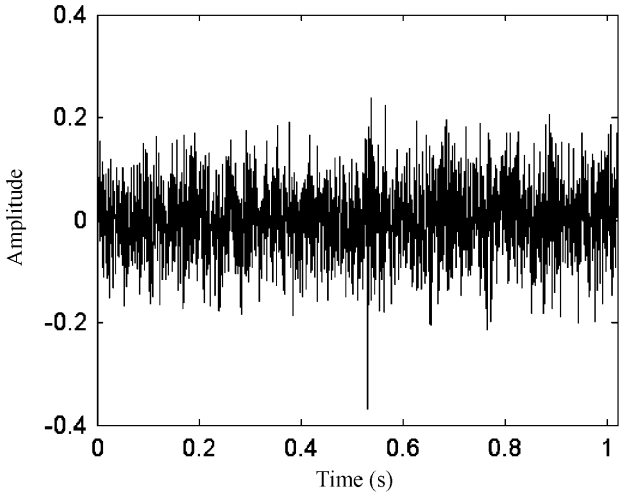

Fig. 5. The simulated signal with additive white noise.

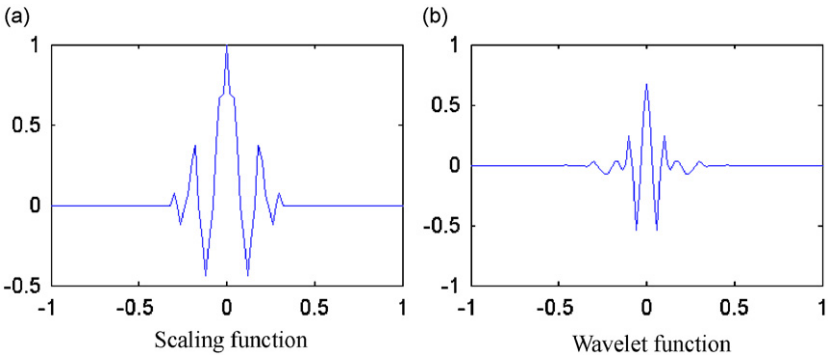

Fig. 6. Scaling function and wavelet function adapted to the signal shown in Fig. 5.

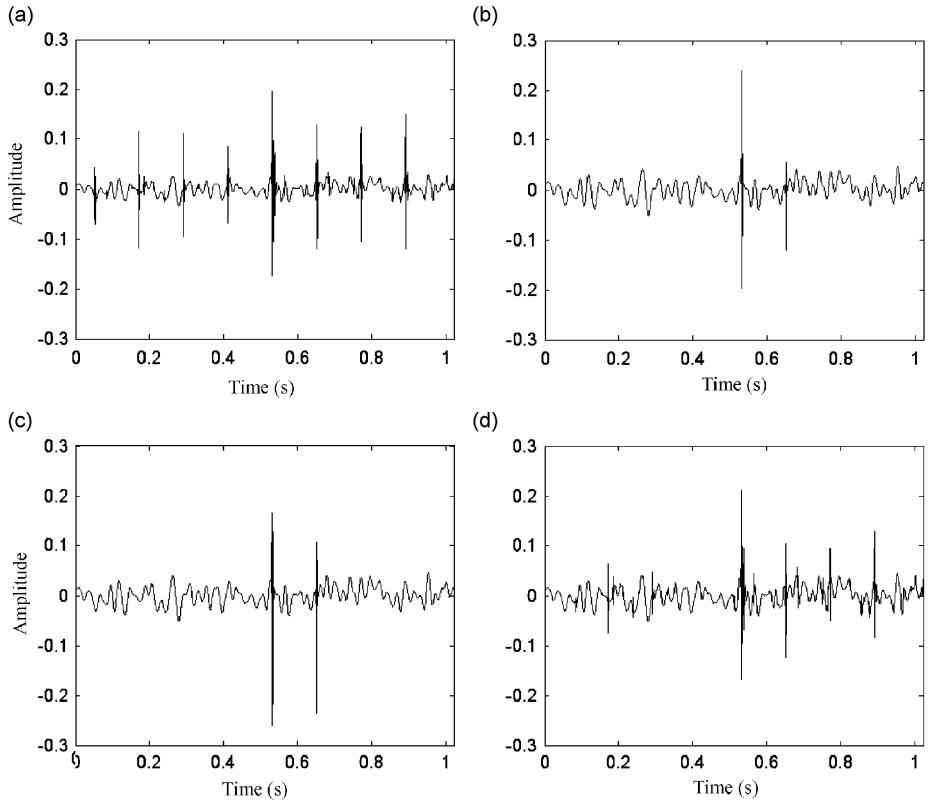

Fig. 7. The purified signals in the simulation experiment using different denoising methods: (a) the purified signal using the proposed method, (b) the purified signal using Donoho's hard-thresholding method, (c) the purified signals using NeighCoeff denoising method, and (d) the purified signal using Donoho's soft-thresholding method.

The results show that the NeighCoeff denoising outperforms the Donoho's hard-thresholding and soft-thresholding for impulse extraction.

Compared with Fig. 7(b)–(d), the results in Fig. 7(a) show that the proposed denoising method is better than the NeighCoeff denoising, Donoho's hard-thresholding and soft-thresholding for the extraction of the periodic impulses.

The noisy signal shown in Fig. 5 is analyzed using the traditional Daubechies 8 wavelet. The purified signals are shown in Fig. 8. The periodic impulses are not extracted effectively.

6.2. *Practical experiments*

Generally, faults that occur in ball or rolling bearings are related to their defective inner-races, outer-races, rolling elements, or cages [29]. Since the measured vibration signals are always complex and non-stationary, and the defect-induced impulses are often buried in background noise. Hence, it is very difficult to distinguish them from noisy signals. To demonstrate the performance of the proposed method for bearing fault detecting, our objective is to extract the impulsive signals related to bearing characteristic frequency from the vibration signals. This section presents two application examples for the detection of localized outer- and inner-race defects. The geometric parameters of the rolling bearing in the experiment are listed in Table 1.

6.2.1. *Case 1: detection of outer-race defects in rolling bearing*

Fig. 9 shows the outer race of bearing with the localized defects. The speed of the spindle is 195 rev/min, that is the rotating frequency $f = 3.25$ Hz. Based on the geometric parameters and rotating speed, the characteristic

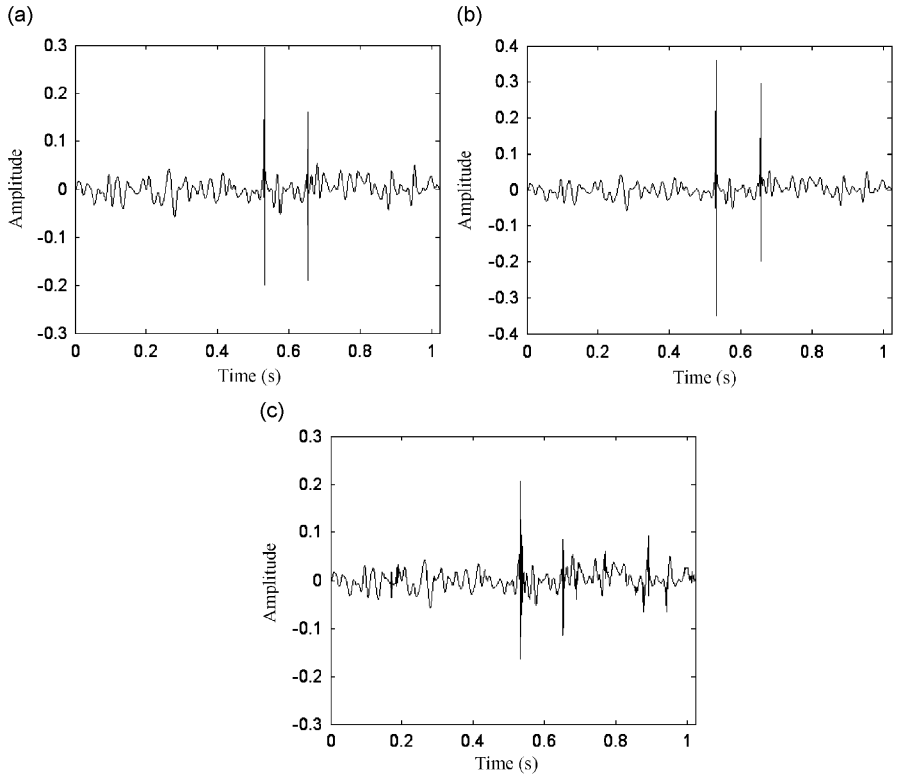

Fig. 8. The purified signals in the simulation experiment using Daubechies 8 wavelet: (a) the purified signal using Donoho's hard-thresholding method, (b) the purified signal using Donoho's soft-thresholding method, and (c) the purified signals using NeighCoeff denoising method.

Table 1
The geometric parameters of the tested bearing

Ball diameter, d	68 mm
Pitch diameter, E	450 mm
Contact angle, α	0°
Number of rolling elements, z	17

frequency of the outer-race defects can be calculated by the following formula:

$$f_o = \frac{1}{2} f \left(1 - \frac{d}{E} \cos \alpha\right) z. \tag{29}$$

Using the above formula, the characteristic frequency of outer-race defects is calculated to be at 23.45 Hz. That is, for outer-race defects, the period of the characteristic impulses is 0.042 s.

The vibration signals are collected from accelerometers mounted on the bearing housing. The signals are digitized at a sampling frequency of 12.8 kHz. Fig. 10 shows the vibration signal of the inspected bearing. According to bearing kinematics and dynamics, an impact occurs each time a roller encounters the spalls. However, from Fig. 10, these impacts are buried in the wideband noise and environmental noise. The fast Fourier transform (FFT) spectrum of vibration signal is shown in Fig. 11. The meaningful information for detecting the outer-race defects is not given in Figs. 10 and 11.

In order to extract the feature components caused by the outer-race defects, we use the customized wavelet denoising based on intra- and inter-scale dependency to analyze the vibration signal shown in Fig. 10. The optimal prediction operator $\boldsymbol{P}_{\text{opt}}$ is [−0.0241, −0.0896, 0.6137, 0.6137, −0.0896, −0.0241], and the optimal

Fig. 9. Bearing with localized outer-race defects.

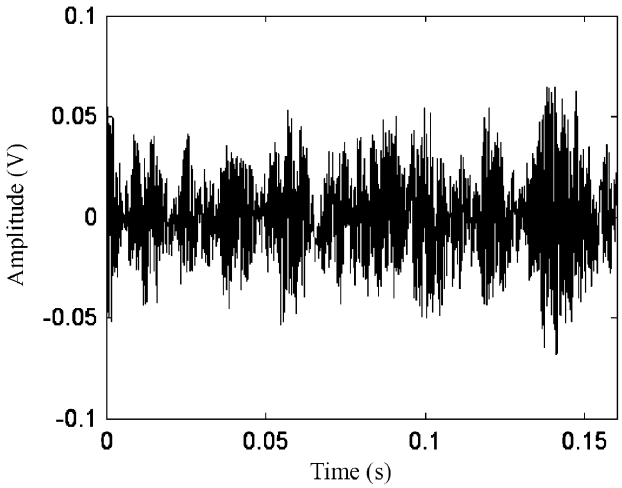

Fig. 10. The vibration signal collected from the bearing with localized outer-race defect.

update operator $\boldsymbol{U}_{\text{opt}}$ is [0.0002, −0.0319, 0.2817, 0.2817, −0.0319, 0.0002]. The customized scaling function and wavelet function are shown in Fig. 12. The vibration signal with outer-race defects is performed 4-level decomposition by redundant lifting scheme, and then the wavelet coefficients are thresholded by our improved algorithm. The purified signal using the proposed denoising method is shown in Fig. 13(a). Evenly spaced impulse clusters can be observed from Fig. 13(a). The periodic interval of the impulse clusters is approximately equal to 0.042 s, which are equivalent to the inverse of the characteristic frequency of outer-race defects (f_o). Hence, it can be concluded that the impulses are caused by the outer-race defects of rolling bearing.

The same signal with localized outer-race defects is analyzed by using the Donoho's hard-thresholding, soft-thresholding, and the NeighCoeff denoising method based on the non-adaptive lifting scheme. The results are shown in Fig. 13(b)–(d). Compared with the waveform shown in Fig. 13(a), the periodic impulses are not extracted obviously in Fig. 13(b)–(d).

To confirm the effectiveness of the proposed method, the vibration signal shown in Fig. 10 is analyzed using the traditional enveloping technique. Fig. 14 illustrates the envelope spectrum of the vibration signal. From Fig. 14, there is not an obvious spectrum line at the characteristic frequency of outer-race defects (23.45 Hz).

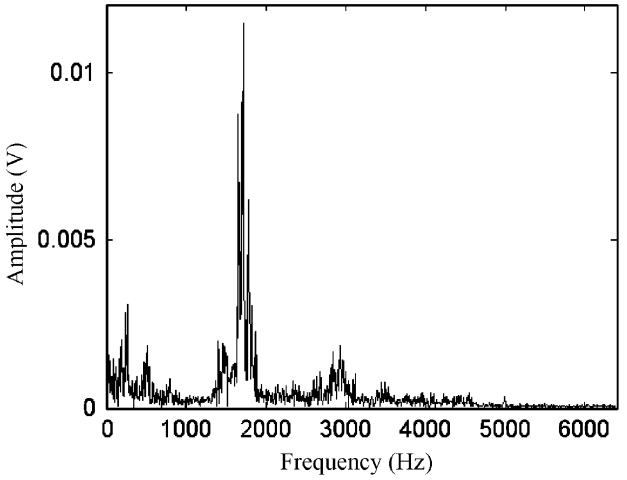

Fig. 11. The FFT spectrum of the vibration signal shown in Fig. 10.

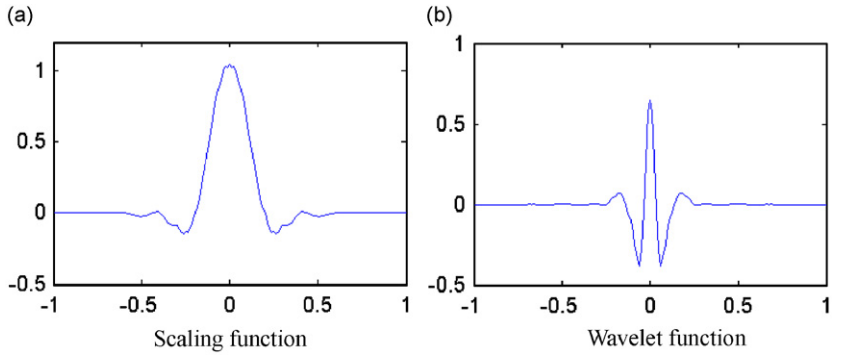

Fig. 12. Scaling function and wavelet function adapted to the vibration signal shown in Fig. 10.

The same vibration signal is also processed using the traditional Daubechies 8 wavelet denoising method. The purified signals are shown in Fig. 15. Compared with the Fig. 13(a), only several impulses are extracted.

6.2.2. Case 2: detection of inner-race defects in roller bearing

Fig. 16 shows the inner race of bearing with the localized defects. The speed of the spindle is 300 rev/min, that is the rotating frequency $f = 5.0$ Hz. Based on the geometric parameters and rotating speed, the characteristic frequency of the inner-race defects can be calculated by the following formula:

$$f_i = \frac{1}{2} f \left(1 + \frac{d}{E} \cos \alpha\right) z. \tag{30}$$

Using the above formula, the characteristic frequency of inner-race defects is calculated to be at 48.92 Hz. That is, for inner-race defects, the period of the characteristic impulses is 0.020 s.

Because inner-race defects have more transfer segments when transmitting the impulse to the outer surface of the bearing housing, the impulse components are rather weak in bearing vibration signal. Fig. 17 illustrates the vibration signal of roller bearing with the localized inner-race defects. The vibration signal is acquired by an accelerometer mounted on the bearing housing. The sampled frequency is 12.8 kHz. From Fig. 17, the periodic impulses related to the inner-race defects are covered by heavy background noise. The FFT spectrum of vibration signal of the inspected bearing is shown in Fig. 18. The useful information for detecting the failure is not given in Fig. 18.

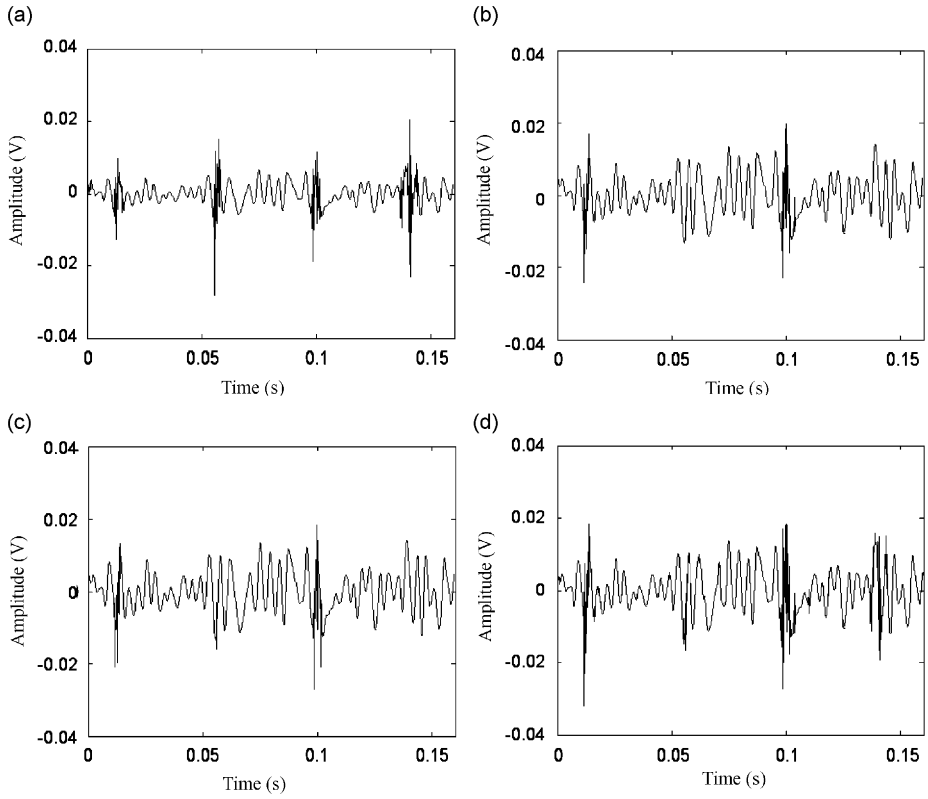

Fig. 13. The purified signals with localized outer-race defects using different denoising methods: (a) the purified signal using the proposed method, (b) the purified signal using Donoho's hard-thresholding method, (c) the purified signal using Donoho's soft-thresholding method, and (d) the purified signals using NeighCoeff denoising method.

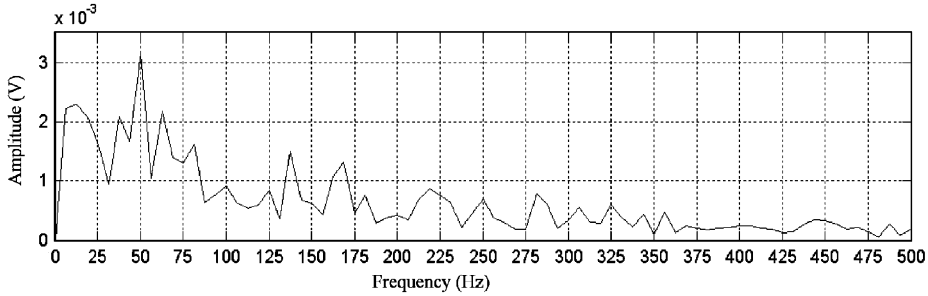

Fig. 14. The envelope spectrum of the signal shown in Fig. 10 using enveloping technique.

In order to extract the feature components caused by inner-race defects, the customized wavelet denoising based on intra- and inter-scale dependency is used to analyze the vibration signal shown in Fig. 17. As introduced in Section 3, the optimal prediction operator $\boldsymbol{P}_{\text{opt}}$ and update operator $\boldsymbol{U}_{\text{opt}}$ are obtained. They are [0.004, −0.2796, 0.7756, 0.7756, −0.2796, 0.004] and [0.0475, −0.0948, 0.2973, 0.2973, −0.0948, 0.0475]. The customized scaling function and wavelet function are shown in Fig. 19. The vibration signal with inner-race defects is performed 4-level decomposition by redundant lifting scheme. Fig. 20(a) shows the purified signal using the proposed denoising method. The periodic impulses appear clearly in Fig. 20(a). The period is just about 0.020 s, which is in accordance with the characteristic frequency of inner-race defects (f_i).

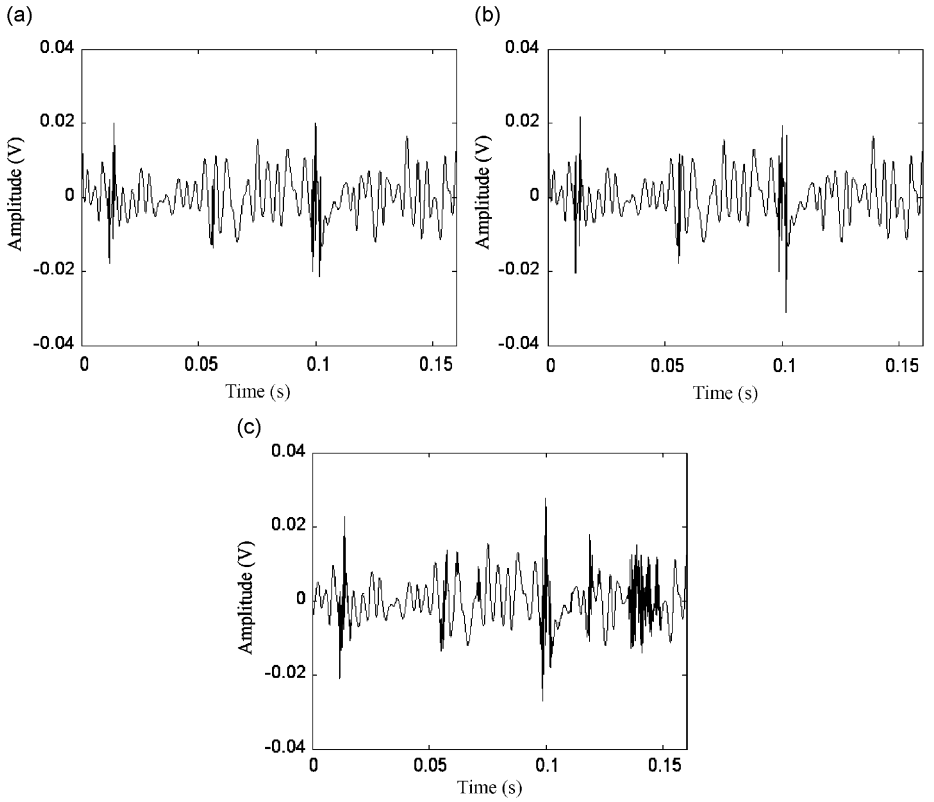

Fig. 15. The purified signals with localized outer-race defects using Daubechies 8 wavelet: (a) the purified signal using Donoho's hard-thresholding method, (b) the purified signal using Donoho's soft-thresholding method, and (c) the purified signals using NeighCoeff denoising method.

Fig. 16. Bearing with localized inner-race defects.

The vibration signal with inner-race defects is also analyzed using the Donoho's hard-thresholding, soft-thresholding and the NeighCoeff denoising method based on the non-adaptive lifting scheme for comparison. The results are shown in Fig. 20(b)–(d). The periodic impulses related to the inner-race defects are not revealed in Fig. 20(b)–(d).

The vibration signal shown in Fig. 17 is analyzed using the traditional enveloping technique. Fig. 21 illustrates the envelope spectrum of the vibration signal. There is not an obvious spectrum line at the

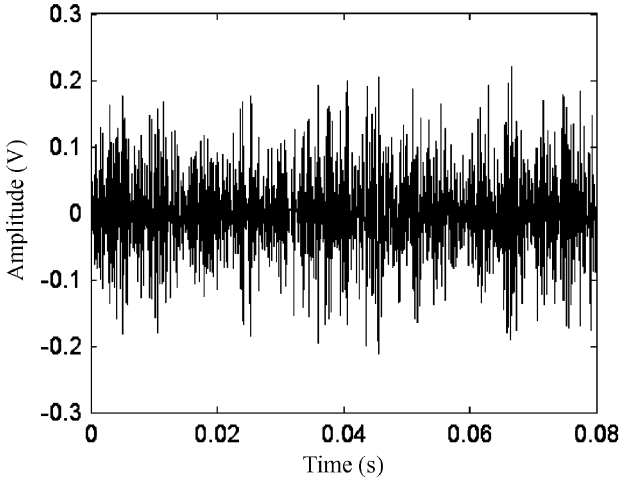

Fig. 17. The vibration signal collected from the bearing with localized inner-race defects.

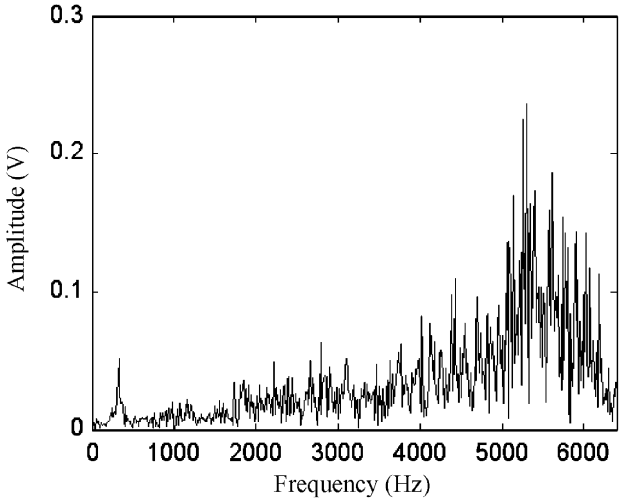

Fig. 18. The FFT spectrum of the vibration signal shown in Fig. 17.

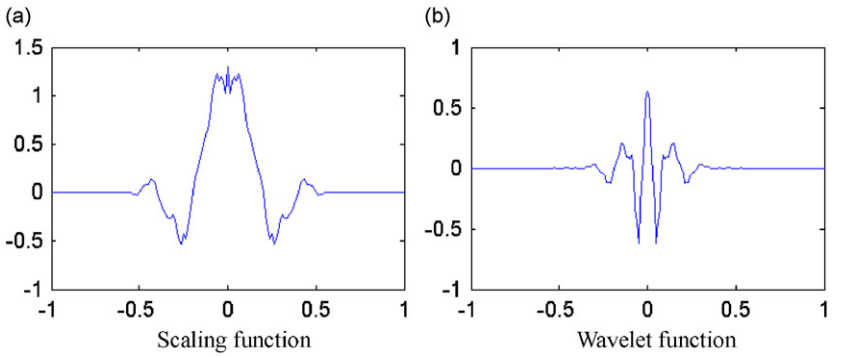

Fig. 19. Scaling function and wavelet function adapted to the vibration signal shown in Fig. 17.

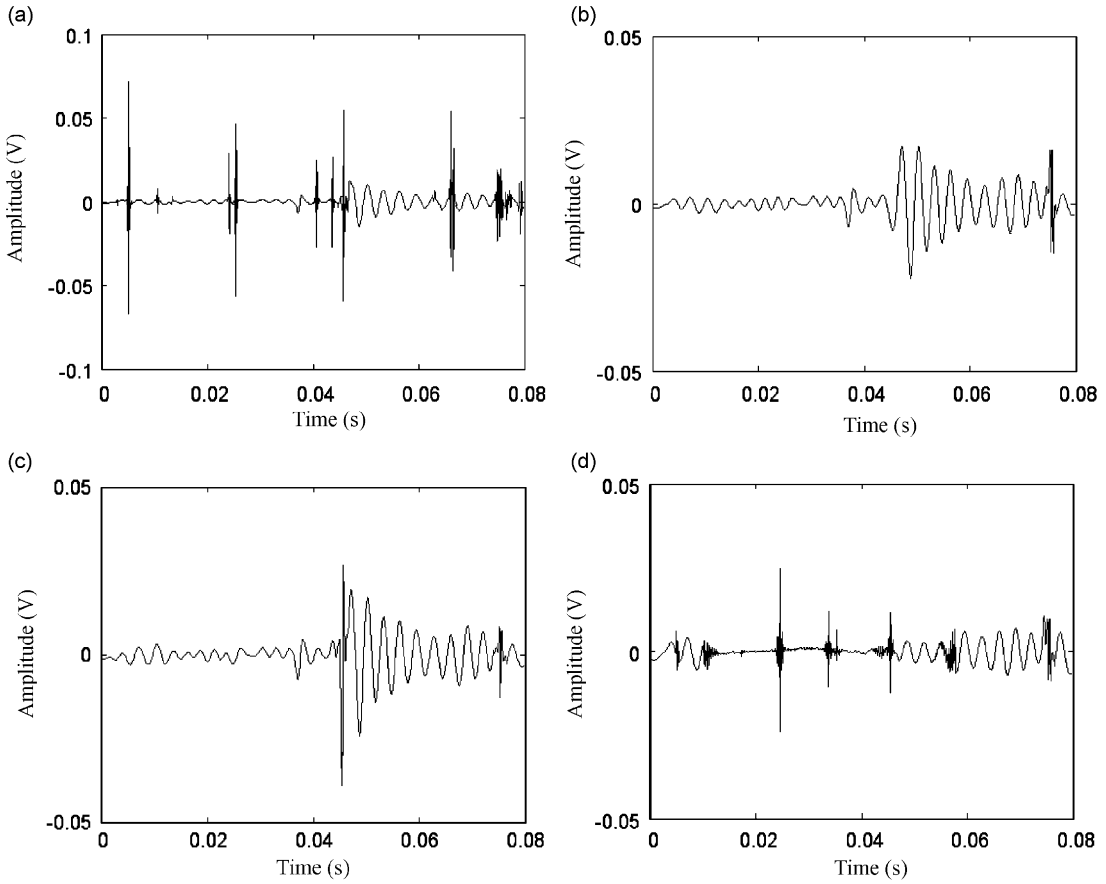

Fig. 20. The purified signals with localized inner-race defects using different denoising methods: (a) the purified signal using the proposed method, (b) the purified signal using Donoho's hard-thresholding method, (c) the purified signal using Donoho's soft-thresholding method, and (d) the purified signals using NeighCoeff denoising method.

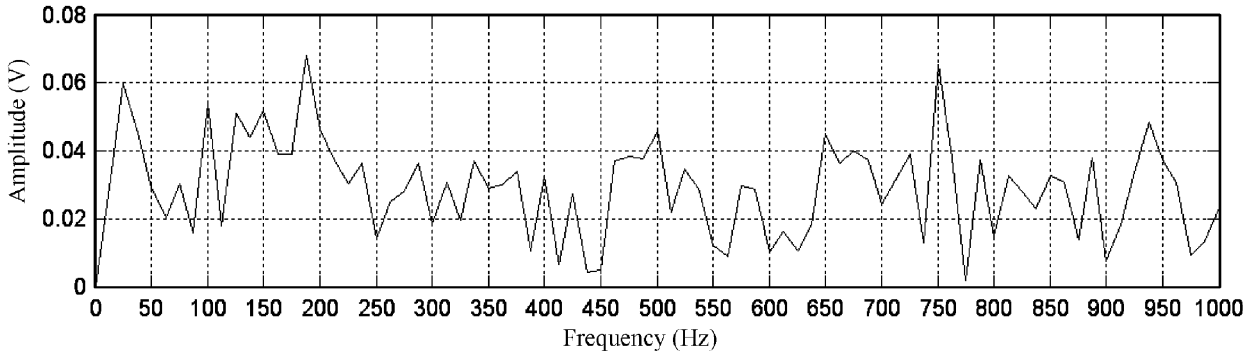

Fig. 21. The envelope spectrum of the signal shown in Fig. 17 using enveloping technique.

characteristic frequency of inner-race defect (48.92 Hz). The same vibration signal is also processed using the traditional Daubechies 8 wavelet denoising method. The purified signals are shown in Fig. 22. None of them can reveal distinctly the fault feature corresponding to the localized inner-race defects.

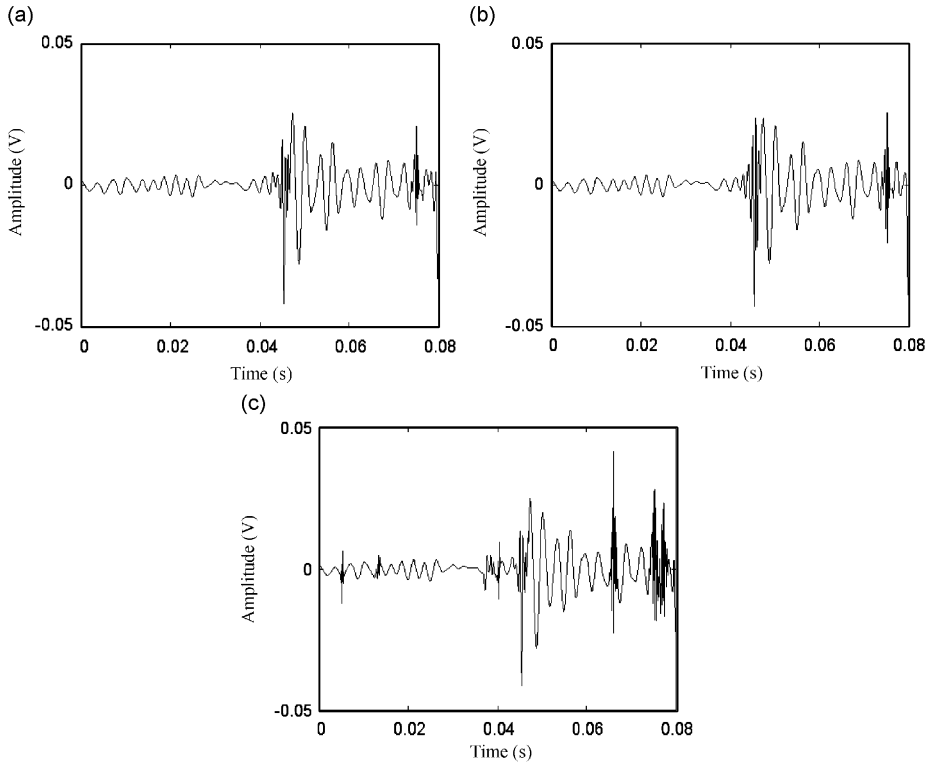

Fig. 22. The purified signals with localized inner-race defects using Daubechies 8 wavelet: (a) the purified signal using Donoho's hard-thresholding method, (b) the purified signal using Donoho's soft-thresholding method, and (c) the purified signals using NeighCoeff denoising method.

7. Conclusion

In this paper, customized wavelet denoising using the intra- and inter-scale dependency of wavelet coefficients has been proposed for bearing fault detection. Firstly, the optimal prediction operator and update operator are designed by the rules of the kurtosis maximization and reconstruction error minimization, respectively. A customized wavelet is constructed, which is adapted to the transient characteristics of the inspected signal. Then, a new denoising method based on customized wavelet is developed by exploiting intra- and inter-scale dependency of wavelet coefficients to improve the NeighCoeff denoising algorithm.

The proposed method has been tested by simulated signal and bearing vibration signals. The results show that it performs better than non-adaptive lifting scheme and traditional Daubechies 8 wavelet that are independent of the inspected signal. Compared with the NeighCoeff denoising, Donoho's hard-thresholding and soft-thresholding, the proposed method clearly extracts the periodic impulse caused by weak fault in rolling bearing. Therefore, it provides an effective method to reveal transient feature components for bearing fault detection.

Acknowledgment

This work was supported by the key project of National Natural Science Foundation of China (No. 50335030), National High-tech R&D Program of China (863 Program) (2006AA04Z430).

References

[1] B.K.N. Rao, *Handbook of Condition Monitoring*, Elsevier Advanced Technology, Oxford, 1996.
[2] R.B.W. Heng, M.J.M. Nor, Statistical analysis of sound and vibration signals for monitoring rolling element bearing condition, *Applied Acoustics* 53 (1998) 211–226.

[3] G.K. Chaturved, D.W. Thomas, Adaptive noise canceling and condition monitoring, *Journal of Sound and Vibration* 76 (3) (1981) 391–405.
[4] P.D. McFadden, J.D. Smith, Vibration monitoring of rolling element bearings by the high frequency resonance technique—a review, *Tribology International* 17 (1) (1984) 3–10.
[5] M. Subrahmanyam, C. Sujatha, Using neural networks for the diagnosis of localized defects in ball bearings, *Tribology International* 30 (10) (1997) 739–752.
[6] T. Liu, J. Singonahalli, N. lyer, Detection of roller bearing defects using expert system and fuzzy logic, *Mechanical Systems and Signal Processing* 10 (5) (1996) 595–614.
[7] J. Lin, L. Qu, Feature extraction based on Morlet wavelet and its application for mechanical fault diagnosis, *Journal of Sound and Vibration* 234 (1) (2000) 135–148.
[8] Y. Shao, K. Nezu, Design of mixture de-noising for detecting faulty bearing signals, *Journal of Sound and Vibration* 282 (2005) 899–917.
[9] Q. Sun, T. Yang, Singularity analysis using continuous wavelet transform for bearing fault diagnosis, *Mechanical Systems and Signal Processing* 16 (6) (2002) 1025–1041.
[10] C.J. Li, J. Ma, Wavelet decomposition of vibrations for detection of bearing—localized defect, *NDT&E International* 30 (3) (1997) 143–149.
[11] P. Tse, Y.H. Peng, R. Yam, Wavelet analysis and envelope detection for rolling element bearing fault diagnosis—their effectiveness and flexibility, *Journal of Vibration and Acoustics—Transactions of the ASME* 123 (3) (2001) 303–310.
[12] W. Sweldens, The lifting scheme: a custom-design construction of biorthogonal wavelets, *Applied Computer Harmonic Analysis* 3 (2) (1996) 186–200.
[13] W. Sweldens, The lifting scheme: a construction of second generation wavelets, *SIAM Journal of Mathematical Analysis* 29 (2) (1997) 511–546.
[14] C. Duan, Z. He, H. Jiang, A sliding window feature extraction method for rotating machinery based on the lifting scheme, *Journal of Sound and Vibration* 299 (2007) 774–785.
[15] H. Jiang, Z. He, C. Duan, P. Chen, Gearbox fault diagnosis using adaptive redundant lifting scheme, *Mechanical Systems and Signal Processing* 20 (2006) 1992–2006.
[16] D.L. Donoho, Denoising by soft-thresholding, *IEEE Transactions on Information Theory* 41 (1995) 613–627.
[17] R.R. Coifman, D.L. Donoho, Translation invariant denoising, in: *Wavelet and Statistics*, *Springer Lecture Notes in Statistics*, Vol. 103, Springer, New York, pp. 125–150.
[18] T.T. Cai, B.W. Silverman, Incorporating information on neighboring coefficients in wavelet estimation, *Sankhya: The Indian Journal of Statistics Series B* 63 (Part 2) (2001) 127–148.
[19] G.Y. Chen, T.D. Bui, Multiwavelets denoising using neighboring coefficients, *IEEE Signal Processing Letters* 10 (2003) 211–214.
[20] Y. Xu, J.B. Weaver, D.M. Healy, J. Lu, Wavelet transform domain filters: a spatially selective noise filtration technique, *IEEE Transactions on Image Processing* 3 (1994) 747–758.
[21] M.S. Crouse, R.D. Nowak, R.G. Baraniuk, Wavelet-based signal processing using hidden Markov models, *IEEE Transactions on Signal Processing* 46 (1998) 886–902.
[22] J. Liu, P. Moulin, Information-theoretic analysis of interscale and intrascale dependencies between image wavelet coefficients, *IEEE Transactions on Image Processing* 10 (2001) 1647–1658.
[23] A. Gouze, M. Antonini, M. Barlaud, B. Macq, Design of signal-adapted multidimensional lifting scheme for lossy coding, *IEEE Transactions on Image Processing* 13 (12) (2004) 1589–1603.
[24] L. Qu, Z. He, *Mechanical Diagnostics*, Shanghai Science and Technology Press, PR China, 1986.
[25] Z. Michalewicz, *Genetic Algorithms+Data Structures = Evolution Programs*, Springer, New York, 1992.
[26] R.L. Claypoole, Adaptive Wavelet Transform via Lifting, PhD Thesis, Department of Electrical and Computer Engineering, Rice University, Houston, TX, October 1999.
[27] E.P. Simoncelli, Bayesian denoising of visual images in the wavelet domain, *Bayesian Inference in Wavelet Based Models*, Springer, New York, 1999, pp. 291–308.
[28] W. Sweldens, P. SchrÖder, Building your own wavelets at home, *Wavelets in Computer Graphics*, *ACM SIGGRAPH Course Notes*, 1996, pp. 15–87.
[29] D. Bently, Predictive maintenance through the monitoring and diagnostic of rolling element bearings, *Applications Note, ANO44*, Bently Nevada Co., 1989, pp. 2–8.